ISSN (Print) 1226-1750
ISSN (Online) 2233-6656
Journal of Magnetics 26(1), 32-40 (2021) https://doi.org/10.4283/JMAG.2021.26.1.032

Vortex Domain Wall Structures and Exchange Coupled Magnetization Switching in Bit Patterned Media

Zijun Wang[1], Ying Zheng[2,3], Wangqiang He[4], Xingqiao Ma[4], and Pingping Wu[2,3]*

[1]*China Institute of Atomic Energy (CIAE), Beijing, Beijing 102413, China*
[2]*Department of Materials Science and Engineering, Xiamen Institute of Technology, Xiamen, Fujian 361021, China*
[3]*The Higher Educational Key Laboratory for Flexible Manufacturing Equipment Integration of Fujian Province, Xiamen Institute of Technology, Xiamen, Fujian 361021, China*
[4]*Department of Physics, University of Science and Technology Beijing, Beijing, Beijing 100083, China*

(Received 26 December 2020, Received in final form 14 March 2021, Accepted 16 March 2021)

After twenty years study of the exchange spring effect, this effect has shown strong potential in application on the perpendicular record process. It satisfies all the necessary properties required by the perpendicular record process. The exchange coupled patterned media also provide a new way to further increase the data storage in the future. Although studies involve many aspects of the exchange spring effect are taken by experiments and theoretical simulations, a systematic study on a magnetic island perpendicular switching for patterned media is not present. We studied the in-plane and out-of-plane switching process with domain wall movement coupling with the finite boundary condition. Many details like magnetic domain wall, coercive field, remanent magnetization and hysteresis loops are discussed to enhance the magnetic device design. An in-plane vortex domain wall was reported in the simulation and the magnetic loops can be artificially designed.

Keywords : exchange coupling, micromagnetic simulation, magnetic vortex, bit patterned media

1. Introduction

Since the perpendicular magnetic recording technology was proposed by Iwasaki and Takemura in 1975 [1], it has been applied in the magnetic recording industry recently [2]. The perpendicular recording mode is an accumulation of the relatively well-aligned easy axis of each magnetic grain in the direction perpendicular to the plane of the disk [3], thus relaxes the stringent requirements of the write field for achieving sharp transitions for conventional longitudinal recording, provides a new technique to reduce the limitation of thermal stability [4], and significantly increase the data storage capacity. However, the demagnetization field generated by the neighboring bit makes the bit smaller. For keeping their memory, it requires a high magnetic anisotropy material to avoid the superparamagnetization effect [5].

Recent years, high magnetic anisotropy materials, such like the tetragonal phase of $L1_0$-FePt, can overcome the superparamagnetic limits and achieve an ultrahigh-density perpendicular media beyond 1 Tbit/in^2 [6, 7]. The magnetocrystalline anisotropy of FePt can reach 5 MJ/m^3. However, this material has a high coercive field of 30 kOe which is impossible for any magnetic write head to write on [8]. A solution for this is the multi-layered exchange spring thin film structure [6, 9, 10]. The presents of the exchange spring media have been proposed to decrease the high switching field of FePt $L1_0$ phase.

To receive higher areal density for the future magnetic recording technology, bit patterned media, which was firstly proposed by New *et al*. [11] and Chou *et al.* [12] in 1994, enables highest potential due to each island contains a single bit of information [13]. The biggest challenge for bit patterned media is the cost-effective production of patterned islands. Alternatively, shingled magnetic recording technology [14] promises areal density beyond 10 Tbit/in^2 whereby data tracks are squeezed by overlapping the written tracks. The lithographic technologies, including optical lithographic [15-17], x-ray lithographic [18, 19], electron beam lithographic [20-22] and the nanoimprint lithographic [23, 24], or the self-assembly method, like template growth [25-27], block co-polymer assembly

©The Korean Magnetics Society. All rights reserved.
*Corresponding author: Tel: +86-592-6667570
Fax: +86-592-6667570, e-mail: pingpingwu-ustb@126.com

[28, 29], and self-assembled nanoparticles [30, 31], can be potentially used to fabricate the patterned magnetic media for future commercial applications.

By employing these manufactory lithographic technologies, bit patterned media has a well-defined bit boundary, which makes its recording process greatly different to conventional recording process. For conventional recording process, the bit boundaries is decided by the magnetic grain boundary, as if the exchange coupling system is introduced, the bit boundary will get very wide. However, for patterned media, as the bit boundaries are fixed, the strong exchange coupling in the magnetic entity of a bit-patterned media does not affect the bit boundary, due to the exchange interaction, the magnetic moments in the magnetic entity coupled strongly to act as a single domain. There are some review articles in this field [32-34].

In the domain structure, domain wall, and in particular the switching process of the exchange coupled system in patterned media, i.e., in a magnetic island structure with fixed boundaries, have not been investigated yet. In terms of the evolution of the magnetic domain structure, such as mandatory field and remanent magnetization, is to describe and understand the focus of the switching process. Jiang *et al.* [35] and Suess *et al.* [36] used theoretical model or micromagnetic simulations to explore the role of internal magnetic structures on the magnetic switching process in exchange coupling systems. Zhang uses Stoner-Wohlfarth model to describe the effect of compressive stress on magnetization of alloys [37]. In the Kim and Kim's micromagnetic simulation [38], they discussed the formation of quasicrystals from the perspective of two different topological charges based on the modeling of magnetic vortices in soft magnetic nanodisks. In the model of Wibowo *et al.* [39], not only the effect of temperature on the magnetization reversal characteristics was studied, but also the effect of spin structure nano dots on the magnetization switch was proposed. At the terms of the application of mass data storage, Goll *et al.* [40-42] started to propose and prove that the stress field of flat plate isolated nanocomposites composed of FePt/Fe structure is lower than that of traditional Exchange Coupled Composites (ECC) structure materials. Additionally, Goll proposed that $L1_0$-FePt's thin film/nanometer point structure not only has the advantages of high density, chemical stability and magnetic stability, but also has the characteristics of low price, which also means that this material is the most promising future product among magnetic recording media materials. Wu *et al.* [43] further studied how the $L1_0$-FePt achieved low obstinacy and high vertical ratio by using the Object-Oriented Micro Magnetic Framework (OOMMF).

Micromagnetic simulations of magnetic domain structures during the switching process in exchange coupled patterned media were performed in this work. Especially the influences of island lateral size, soft/hard layers ratio, island shape and stacking structure on the remanence and coercivity of hysteresis were simulated. We also studied the domain wall structure in the exchange coupled islands, a three-dimension vortex domain wall structure was observed in the switching process in the present study. Moreover, if the external magnetic field was applied along [100] or [110] directions, the exchanged coupled islands exhibit a constricted or a stretched loop, the switching characteristic of these domain structures becomes even more dramatic.

2. Simulation Method

To reveal the domain structures for patterned media, the magnetization vector M_i (i = 1, 2, 3) is chosen as order parameter. The three-dimensional micromagnetic simulation is carried out by solving the Landau-Lifshitz-Gilbert (LLG) equations numerically:

$$(1+\alpha^2)\frac{\partial M}{\partial t} = -\gamma_0 M \times H_{eff} - \frac{\gamma_0 \alpha}{M_s} \times (M \times H_{eff}), \quad (1)$$

where α is the damping constant, γ_0 is the gyromagnetic ratio, M_s is the saturation magnetization, and H_{eff} is the effective magnetic field

$$H_{eff} = -\frac{1}{\mu_0}\frac{\partial E}{\partial M}, \quad (2)$$

where μ_0 is the permeability of vacuum, E is the total free energy in magnets, in this work, we take into account four energetic contributions, thus the total free energy is given by

$$E = E_{anis} + E_{exch} + E_{ms} + E_{zeeman}, \quad (3)$$

where E_{anis}, E_{exch}, E_{ms}, and E_{zeeman} are magnetocrystalline anisotropy, magnetic exchange, magnetostatic and Zeeman energies, respectively.

The anisotropy energy for a cubic magnetic crystal is given by

$$E_{anis} = \int \left[K_1 \left(m_1^2 m_2^2 + m_1^2 m_3^2 + m_2^2 m_3^2 \right) + K_2 m_1^2 m_2^2 m_3^2 \right] dV, \quad (4)$$

where K_1, K_2 are anisotropy constants, m_i are the components of unit magnetization vector, i.e., $m_i = M_i/M_s$. V is the total volume. The exchange energy is determined solely by the spatial variation of the magnetization orientation and can be written as:

$$E_{exch} = A \int (\nabla m)^2 dV, \quad (5)$$

where A is the exchange stiffness constant. To calculate the magnetostatic interaction energy, we used a convolution of magnetization with the three-dimensional LaBonte interaction matrix, the analytic formula developed by Schabes and Aharoni [44] is written in the form

$$E_{ms} = \frac{1}{2}\Sigma'_{ijk,i'j'k'} E_{ijk,i'j'k'} . \quad (6)$$

The details of the calculations of magnetostatic energy for the fixed boundary magnets can be obtained from Ref. [45].

The Zeeman energy is taken into account through the interaction between the magnetization and the external field H_{ex}:

$$E_{zeeman} = -\mu_0 M_s \int H_{ex} \cdot m dV . \quad (7)$$

The temporary evolution of the magnetic domain structure and the magnetization vector map are obtained by solving Eq. (1) numerically with Gauss-Seidel projection method [46].

3. Results and Discussions

3.1. Typical hysteresis loops of FePt/Fe exchange spring media and the vortex domain wall structure

We first consider a FePt/Fe bilayer magnetic island with a system size of $8\Delta x \times 8\Delta x \times 64\Delta x$, where $\Delta x \sim 4$ nm is the simulation grid spacing. The thickness of the hard layer and soft layer were both $32\Delta x$. For the FePt layer, the saturation magnetization $M_{sh} = 1.050 \times 10^6$ A/m, the anisotropy constants $K_{1h} = 1.7 \times 10^6$ J/m^3, $K_{2h} = 0$ J/m^3, and exchange stiffness constant $A_h = 10^{-11}$ J/m; For the iron layer, the corresponding parameters are assumed to be $M_{ss} = 1.575 \times 10^6$ A/m, $K_{1s} = 4.7 \times 10^4$ J/m^3, $K_{2s} = 0$ J/m^3, and $A_s = 10^{-11}$ J/m. For the damping constant in the LLG equation, a value of $\alpha = 1.0$ is used in this simulation. The schematic figure of the system is shown in Fig. 1(a), the initial domain structure was polarized along [001] direction at a field of 3×10^5 A/m. We decreased the external field to -3×10^5 A/m by a step of 5 kA/m, then reverse its direction and created the hysteresis loop. A typical exchange coupled hysteresis is presented in Fig. 1(b); a discontinuity in the slope of the demagnetization curve can be clearly seen. The magnetization sharply decreased to zero at –250 kA/m, then slowly reaches full saturation.

To understand the relationship between the domain structure and the demagnetization loop, a sequence of magnetic domain structure evolution during the switching process are demonstrated in Fig. 1(c). The domain structures c1-c8 are corresponding to the points 1-8 in the hysteresis loop, respectively. It is interesting to note that a vortex shape domain structure was observed at the top of the soft layer when the magnetization starts to decrease, as seen in Fig. 1(c2). With the decrease in the external field, the vortex structure grows and lead to the decrease of the magnetization, however, '-z' domain was not observed in this stage (Fig. 1(c3)). Further decrease the external field, the '-z' domain nucleates and grows with the vortex structure moves to the soft/hard layer interface (Fig. 1(c4)), and hence the magnetostatic energy could be reduced. At a magnetic field of –250 kA/m the soft layer was switched to [00$\bar{1}$] direction, and the vortex structure stays at the soft/hard interface (Fig. 1(c5)). In the following switching process, the vortex domain wall movement produced changes in total magnetization, noted that the thickness of the vortex domain wall was reduced to 20

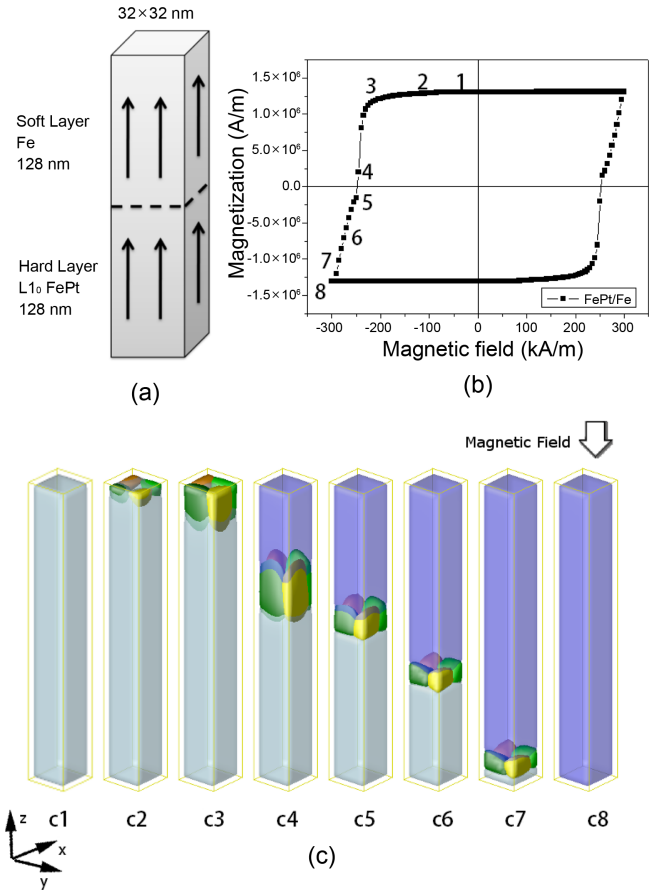

Fig. 1. (Color online) (a) A schematic of the exchange coupled island employed in the simulation. (b) A typical exchange spring hysteresis loop of the exchange coupled island. (c) The magnetic domain structure evolution during the reversal process, the yellow, orange, green, dark green, light blue, and dark blue color represent domains with the magnetization along +x, –x, +y, –y, +z, and –z directions. c1-c8 are corresponding to the point 1-8 in Fig. 1(b), respectively.

nm. The whole system reaches full saturation at a field of –300 kA/m, only '-z' domain was observed in the final domain structure (Fig. 1(c8)). The vortex domain wall structure also could be observed in the nanowire or nanotubes. However, the details of the domain wall structure in the exchanged coupled systems are less reported. Fig. 2(a-c) shows the vector distributions in the cross-section view and the magnetizations along the first column during the switching process. When the switching process starts in the soft layers, it is seen a thick domain walls across the soft layer, the thickness is around 80 nm (20 grids). At a field of –250 kA/m, the domain wall moves to the hard/soft layers interface. An unsymmetrical domain wall was observed. As seen in Fig. 2(b), the magnetization slowly rotates to x direction in the soft layer with a domain wall thickness of 50 nm, then quickly switched to -z direction in the hard layer, and the domain wall thickness is reduced to only 20 nm.

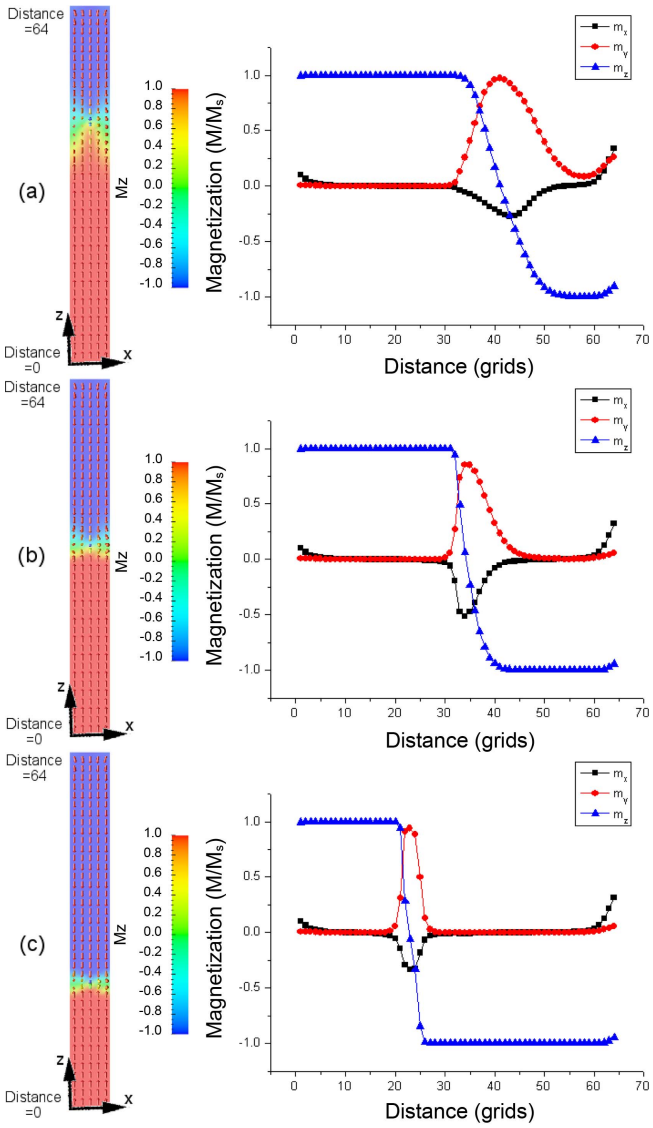

Fig. 2. (Color online) Left: Cross-sectional vector map of the exchange coupled island, (a-c) are corresponding to the domain structure of Fig. 1(c4-c7). Right: The magnetization along the x, y, z direction for the first column of the vector map.

3.2. Lateral Size effect

The magnetization switching process of exchange coupled islands with lateral size of 64 nm and 128 nm were also studied. Different hysteresis loops were obtained as shown in Fig. 3a. Further increase the lateral size of the islands, very small changes were obtained in the coercive field. It is interesting to see that the magnetization starts to decrease earlier for large sized magnetic islands, which implying that the vortex structures is easier

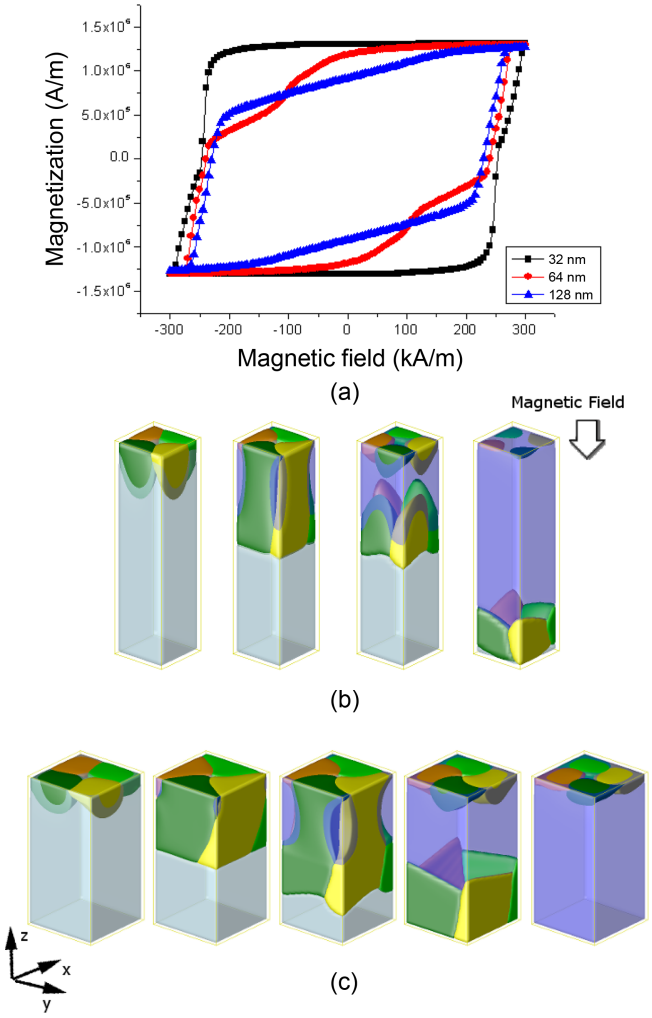

Fig. 3. (Color online) (a) Hysteresis loops for exchange coupled island with lateral size of 32 nm, 64 nm, and 128 nm, (b, c) Magnetic domain evolution during the switching process with the lateral size of 64 nm and 128 nm respectively.

to nucleate due to the decrease of the demagnetization field. It should be noted that the formation of the vortex arises from in-plane magnetization due to the in-plane demagnetization field. In the in-plane direction, with the increase of the size of the magnetic island, the demagnetization field decreases, and lead to the vortex structure nucleation earlier. We also note that the domains firstly nucleate at four corners for large size islands, as seen in Fig. 3b and Fig. 3c. When the size of the island was extended to 128 nm, the magnetization starts to decrease at a positive field of 180 kA/m, and the demagnetization process can be separated into two stages: in the first stage, the vortex domain structure nucleates and grows in the soft layer, as seen in Fig. 3a, which slowly reduced the total magnetization; in the next stage, the nucleation and growth of '-z' domain led to a drastically decrease in the magnetization. The whole hysteresis loops show a parallelogram-liked shape, implying this effect can be potentially employed on the design of magnetic drivers.

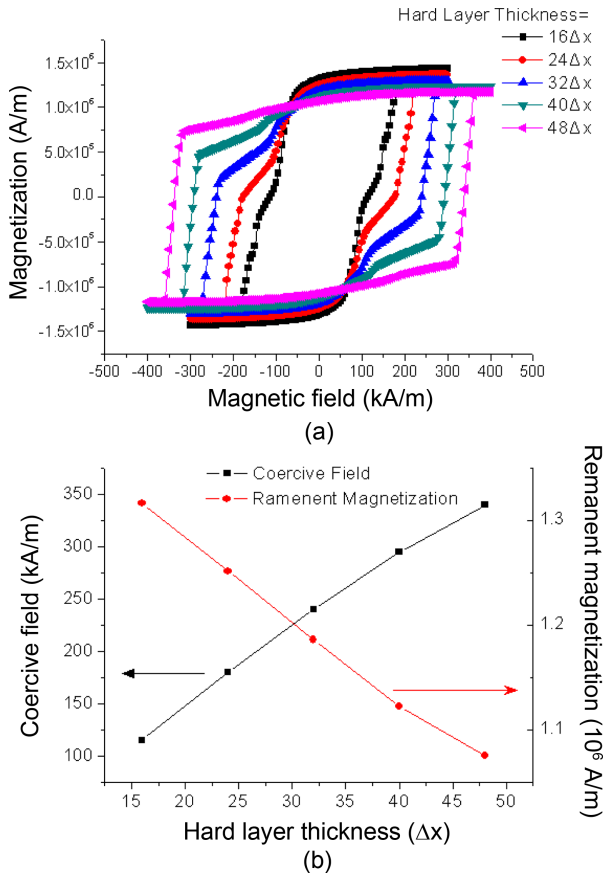

Fig. 4. (Color online) (a) Hysteresis loops for different exchange spring magnets with hard layer thickness of 16Δx, 24Δx, 32Δx, 40Δx, and 48Δx. (b) Plot for simulated coercive field in exchange coupled island as a function of hard layer thickness.

3.3. Coercive field design by adjusting ratio

Adjusting the coercivity of magnets has become a feasible method to design new functional magnetic materials. In order to design a switching-able magnetic island for patterned media, an adjustable coercive field material is a good option. For double-layered exchange spring structures, the coercive field can be easily adjusted by change the ratio of the hard/soft layers.

To examine the influence of the hard/soft ratio on the coercive field of the exchange spring magnets, we fixed the total thickness of the bi-layered structure, and adjusted the thickness of the hard layer. Five hysteresis loops for different exchange spring magnets with hard layer thickness of 16Δ*x*, 24Δ*x*, 32Δ*x*, 40Δ*x*, and 48Δ*x* are presents in Fig. 4(a). All these hysteresis loops exhibit exchange spring behavior. It is interesting to observe that unlike the coercive field, the remanent magnetization has minor changes as the hard/soft ratio varies. Simulation results show that a small amount of domains were seen on the top of the soft layer to decrease the demagnetization energy.

To investigate the relationship between the coercive field and the exchange coupled structure, we plot the coercive field and ramanent magnetization versus hard layer thickness in Fig. 4(b). Quite remarkably, the coercive field, varies from −100 kA/m to −350 kA/m, linearly changes with the thickness of the hard layers. This coercive field-controlled exchange spring magnetic islands suggest a pathway for the design and implementation of patterned media storage devices.

3.4. Triple layer structures

Triple layer exchange spring magnets can be also used for perpendicular recording media, which have advantages on achieving high signal-noise ratio and signal stability [47, 48] or facilitate the fabrications and to improve magnetic switching properties [6]. Triple layer also can be used in the field of thermally assistant exchange spring media [49], micro-electro-mechanical system (MEMS) [35] and spintronics [50]. The unitization of the triple layered exchange systems for the patterned media also requires an understanding of the magnetic switching properties and the related magnetization distributions for enhanced properties.

The comparison of the hysteresis loops of classical bi-layer structure, hard-soft-hard structure, and soft-hard-soft structure illustrate several interesting features about the loop shape (Fig. 5(a)). The hard/soft ratios for all these structures are kept at 1, i.e., the fraction of the hard and soft layers is the same. Loop for hard-soft-hard triple layers (blue triangle) has smaller remanent magnetization

but higher coercive field than traditional bilayer structure (black square). The hard-soft-hard layer has smaller nucleation field due to bi-vortex structure nucleated in one soft layer with different handedness directions for reduced the demagnetization field, as shown in Fig. 5(b). Further increase the magnetic field accelerate the speed of the decrease of the magnetization, which is because two magnetic domain wall moves simultaneously. Compared to bilayer structure, there is no obvious jump for the soft layer switching process due to there is no room for two vortex structure grows. The coercive field is higher means that the two-vortex domain wall motion prevent the growth of the '-z' domain.

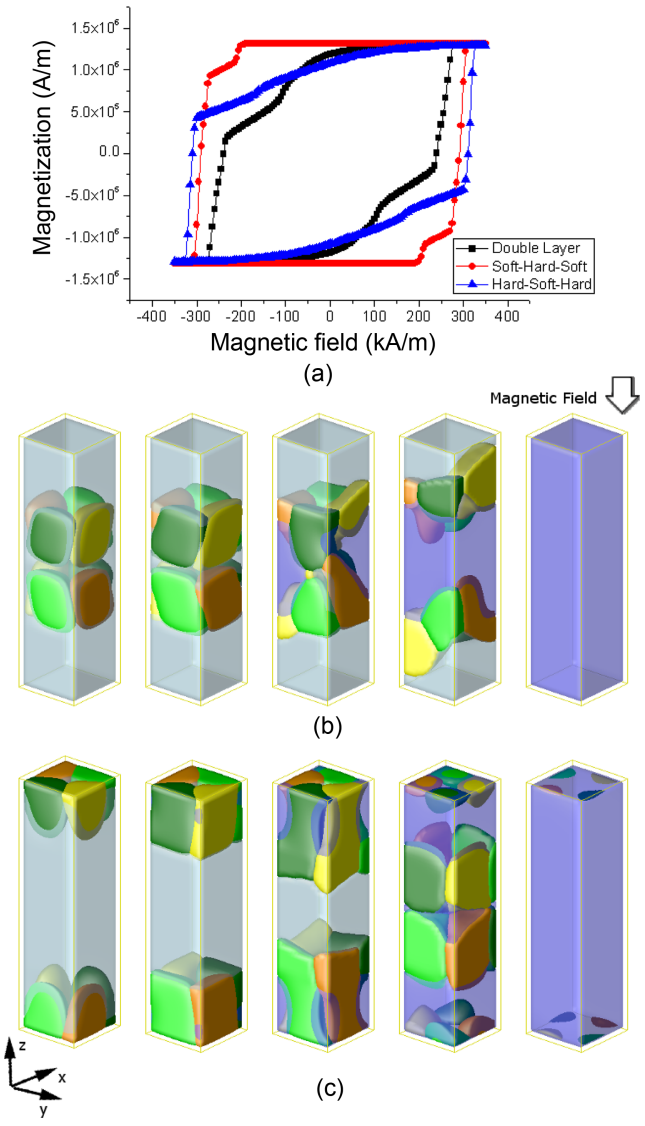

Fig. 5. (Color online) (a) Hysteresis loops for triple layered exchange spring structure. (b-c) Domain evolutions of Hard-Soft-Hard and Soft-Hard-Soft triple layered exchange coupled island.

For soft-hard-soft structure, it's shown that a very high nucleation field as it requires two vortex structures nucleated at both side of the island. The soft layer switching process is similar to bilayered structure, as we can see the domain wall moving in both soft layers, as shown in Fig. 5(c). The loop shows a higher coercive field than bilayer structures. This can be explained by the domain structure, as we can see in Fig. 5(c). Two vortex structures with different handedness meet at the center of the hard layer, which prevents the demagnetization field and increase the coercive field. We also noticed that the core magnetization firstly switched through the triple layer structure near coercive field, and in the following stage, the magnetization of the in-plane vortex rotated toward to the -z direction quickly.

3.5. Shape Effect in a non-magnetic matrix

Using a non-magnetic matrix, the shape of the magnetic island can be assumed to be any shape in the simulation. The magnetic properties of circle-, square-, and rectangle-shaped exchange coupled bi-layered magnetic island in a non-magnetic matrix were studied. Fig. 6 shows the hysteresis loops of the three different shaped magnetic islands. Compared to the original hysteresis loop for square- shaped island with no matrix in 3.1, we observed similar hysteresis for the circle- and square- shaped island. The simulation results show that a non-magnetic matrix has little influence on the hysteresis and the domain structure of exchange coupled system throughout the magnetization switching process.

3.6. In-plane and Out-of-plane exchange effects in bi-layered magnetic island

For a conventional exchange spring structure, the in-plane magnetization switching can be used in longitude

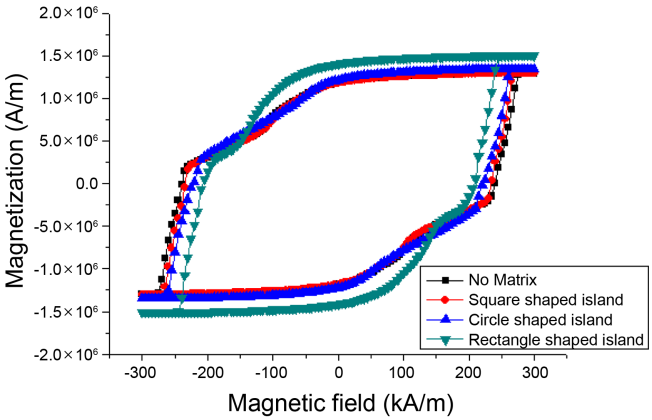

Fig. 6. (Color online) Magnetic hysteresis for exchange coupled islands in different shaped matrix.

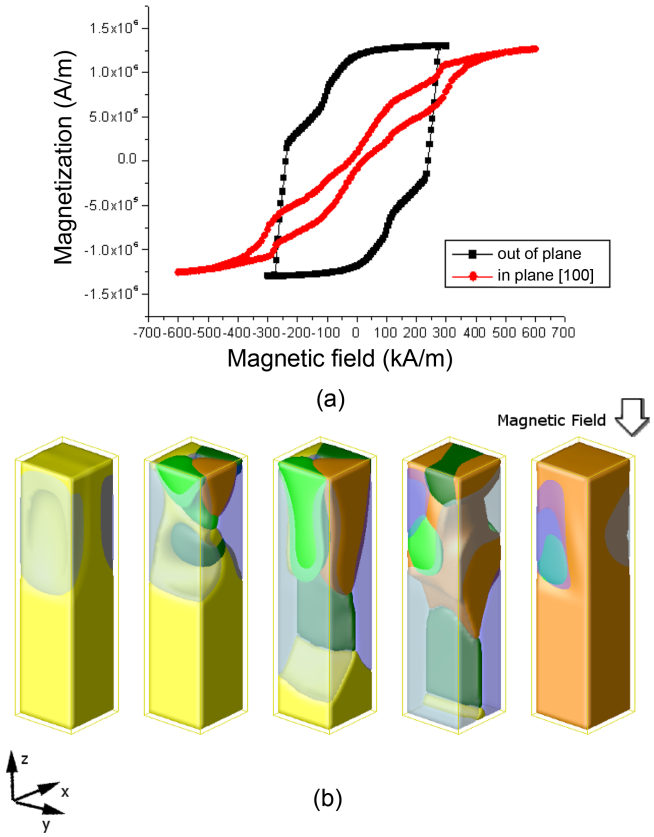

Fig. 7. (Color online) (a) Comparison of hysteresis loops with external field applied along [001] and [100] direction. (b) Magnetic domain evolution during switching process with applied field along [100] direction.

magnetic recording process. Compared to conventional exchange spring effect, we performed a micromagnetic study on the free-standing exchange coupled island to investigate the influence of the fixed boundary on the switching process of the exchange spring structure. In plane switching technology of exchange coupled magnets have numerous applications, including spin configuration [35, 51, 52], spin-flop transitions [53], and negative coercive fields [54, 55].

Two types of hysteresis loops are presented in Fig. 7(a), classified by the direction of external field: in-plane easy axis [100] and perpendicular [001] direction. Please note that the domain structure in the simulation was initially polarized along the in-plane [100] direction. Compared to previous perpendicular switching loops, in-plane hysteresis loops show very narrow hysteresis due to the strong demagnetization field induced by size effect of the magnetic island. A double hysteresis magnetization loop is observed when a magnetic field is applied along the [100] direction, both the remanent magnetization and coercive field return to zero when applied field is completely removed.

To understand the improper coercive field and remanent magnetization, we analyzed the domain structures during the switching process, as shown in Fig. 7(b). With the decrease in the external field, the z domains first nucleate at the side of the magnetic island, with a further decrease in magnetic field, the domain wall motion take place and a vortex structure is observed on the top of the soft layer. When the applied field return to zero, we observed a vortex structure on the top the soft layer and a ‘z/-z’ domain structure, separated by a 180 degree Bloch wall in the hard layer, which lead the remanent magnetization back to zero. When the magnetic field was applied in the opposite direction, the magnetization in the soft layer is switched to -x direction firstly, and then the magnetization switching in the hard layer occurs with a jump in the magnetization. Finally, the magnetization of the exchange coupled system is switched to the -x direction.

4. Summary

We reported studies of magnetization switching process in exchange coupled island for bit patterned media by using micromagnetic simulation. A vortex domain wall structure appears during the switching process. It was found that the magnetic vortex nucleation, growth and movement will lead the magnetization change during the switching process. The effects of lateral size of the island, the soft/hard ratio, triple layered structure, non-magnetic matrix, and in-plane external field on the switching process are also investigated in this work. These results indicate that the magnetic properties of exchanged couple island, including the hysteresis loop, remanent magnetization, and coercive field are strongly influenced by these factors. It is shown that one can also design the exchange coupled magnetic island by changing its geometric structure and the soft/hard ratio. This work opens a new avenue to designing exchange coupled magnetic bit in patterned media to realize high density storage devices at the nanoscale. It also provides a framework for exploring new magnetic materials and new exchange coupled structures to control the magnetic switching process in order to achieve functional magnetic applications in the future.

Acknowledgement

This work was supported by National Key Research and Develop Program of China (Grant No. 2017YFA0403704) and National Natural Science Foundation of China (Grant No. 12075320, 11275274 and 11174030), The author P.

Wu gratefully acknowledge the support of outstanding young research talents program (2016) in colleges and universities of Fujian province, the Cultivating Research Program of Xiamen Institute of Technology 2018, and the Joint Research Program of Xi'an Jiaotong University and Xiamen Institute of Technology with contract No. IPE20190802 (Grant No. IMT2019001). We also would like to thank Dr. Jingxian Zhang and Dr. Long-Qing Chen at Pennsylvania State University for the use of the Micromagnetic Programming code.

References

[1] S. Iwasaki and K. Takemura, IEEE Trans. Magn. **11**, 1173 (1975).
[2] S. Iwasaki, J. Magn. Magn. Mater. **324**, 244 (2012).
[3] S. Khizroev and D. Litvinov, J. Appl. Phys. **95**, 4521 (2004).
[4] Y. Song, D. Zhu, High density data storage: Principle, World Scientific, Singapore (2009).
[5] R. E. Rottmayer, S. Batra, D. Buechel, W. A. Challener, J. Hohlfed, Y. Kubota, L. Li, B. Lu, C. Mihalcea, K. Mountfield, K. Pelhos, C. Peng, T. Rausch, M. A. Seigler, D. Weller, and X. M. Yang, IEEE Trans. Magn. **42**, 2417 (2006).
[6] R. H. Victora and X. Shen, IEEE Trans. Magn. **41**, 537 (2005).
[7] D. Suess, T. Schrefl, S. Fahler, M. Kirschner, G. Hrkac, F. Dorfbauer, and J. Fidler, Appl. Phys. Lett. **87**, 012504 (2005).
[8] V. Alexandrakis, T. Speliotis, E. Manios, D. Niarchos, J. Fidler, J. Lee, and G. Varvaro, J. Appl. Phys. **109**, 07B729 (2011).
[9] F. Casoli, F. Albertini, S. Fabbrici, C. Bocchi, L. Nasi, R. Ciprian, and L. Pareti, IEEE Trans. Magn. **41**, 3877 (2005).
[10] J. P. Wang, W. K. Shen, J. M. Bai, R. H. Victora, J. H. Judy, and W. L. Song, Appl. Phys. Lett. **86**, 142504 (2005).
[11] R. M. H. New, R. F. W. Pease, and R. L. White, J. Vac. Sci. Technol. B **12**, 3196 (1994).
[12] S. Y. Chou, M. S. Wei, P. R. Krauss, and P. B. Fischer, J. Appl. Phys. **76**, 6673 (1994).
[13] M. A. Bashir, T. Schrefl, J. Dean, A. Goncharov, G. Hrkac, D. A. Allwood, and D. Suess, J. Magn. Magn. Mater. **324**, 269 (2012).
[14] R. Wood, M. Williams, A. Kavcic, and J. Miles, IEEE Trans. Magn. **45**, 917 (2009).
[15] A. Fernandez, P. J. Bedrossian, S. L. Baker, S. P. Vernon, and D. R. Kania, IEEE Trans. Magn. **32**, 4472 (1996).
[16] Y. Hao, F. J. Castano, C. A. Ross, B. Vogeli, M. E. Walsh, and H. I. Smith, J. Appl. Phys. **91**, 7989 (2002).
[17] T. A. Savas, M. Farhoud, H. I. Smith, M. Hwang, and C. A. Ross, J. Appl. Phys. **85**, 6160 (1999).
[18] H. I. Smith, J. Vac. Sci. Technol. B **13**, 2323 (1995).
[19] C. Miramond, C. Fermon, F. Rousseaux, D. Decanini, and F. Carcenac, J. Magn. Magn. Mater. **165**, 500 (1997).
[20] C. A. Ross, Annu. Rev. Mater. Sci. **31**, 203 (2001).
[21] J. I. Martin, J. Nogues, K. Liu, J. L. Vicente, and I. K. Schullerc, J. Magn. Magn. Mater. **256**, 449 (2003).
[22] J. C. Lodder, J. Magn. Magn. Mater. **272**, 1692 (2004).
[23] S. Y. Chou, P. R. Krauss, and P. J. Renstrom, Science **272**, 85 (1996).
[24] S. Y. Chou, P. R. Krauss, and P. J. Renstrom, Appl. Phys. Lett. **67**, 3114 (1995).
[25] S. Kawai and R. Ueda, J. Electrochem. Soc. **122**, 32 (1975).
[26] P. Aranda and J. M. Garcia, J. Magn. Magn. Mater. **249**, 214 (2002).
[27] Z. B. Zhang, D. Gekhtman, M. S. Dresselhaus, and J. Y. Ying, Chem. Mater. **11**, 1659 (1999).
[28] J. Y. Cheng, C. A. Ross, V. Z. H. Chan, E. L. Thomas, R. G. H. Lammertink, and G. J. Vancso, Adv. Mater. Formation of a cobalt magnetic dot array via block copolymer lithography **13**, 1174 (2001).
[29] J. Y. Cheng, C. A. Ross, E. L. Thomas, H. I. Smith, and G. J. Vancso, Appl. Phys. Lett. **81**, 3657 (2002).
[30] S. Sun, C. B. Murray, D. Weller, L. Folks, and A. Moser, Science **287**, 1989 (2000).
[31] D. Weller, A. Moser, L. Folks, M. E. Best, L. Wen, M. F. Toney, M. Schwickert, J. U. Thiele, and M. F. Doerner, IEEE Trans. Magn. **36**, 10 (2000).
[32] T. R. Albrecht, H. Arora, V. Ayanoor-Vitikkate, J. M. Beaujour, D. Bedau, D. Berman, A. L. Bogdanov, Y. A. Chapuis, J. Cushen, E. E. Dobisz, G. Doerk, H. M. Grobis, B. Gurney, W. Hanson, O. Hellwig, T. Hirano, P. O. Jubert, D. Kercher, J. Lille, Z. Liu, C. M. Mate, Y. Obukhov, K. C. Patel, K. Rubin, R. Ruiz, M. Schabes, L. Wan, D. Weller, T. W. Wu, and E. Yang, IEEE Trans. Magn. **51** 0800342 (2015).
[33] S. N. Piramanayagam and K. Srinivasan, J. Magn. Magn. Mater. **321**, 485 (2009).
[34] H. Wang, H. Zhao, T. Rahman, Y. Isowaki, Y. Kamata, T. Maeda, H. Hieda, A. Kikitsu, and J. P. Wang, IEEE Trans. Magn. **49**, 707 (2013).
[35] J. S. Jiang, J. E. Pearson, Z. Y. Liu, B. Kabius, S. Trasobares, D. J. Miller, S. D. Bader, D. R. Lee, D. Haskel, G. Srajer, and J. P. Liu, J. Appl. Phys. **97**, 10K311 (2005).
[36] D. Suess, J. Lee, J. Fidler, and T. Schrefl, J. Magn. Magn. Mater. **321**, 545 (2009).
[37] H. Zhang, Appl. Phys. Lett. **98**, 232505 (2011).
[38] J. Kim and S. K. Kim, J. Magn. **22**, 29 (2017).
[39] N. A. Wibowo, D. B. Nugroho, and C. A. Riyanto, J. Magn. **24**, 17 (2019).
[40] D. Goll and S. Macke, Appl. Phys. Lett. **93**, 152512 (2008).
[41] D. Goll and A. Breitling, Appl. Phys. Lett. **94**, 052502 (2009).
[42] D. Goll and T. Bublat, Phys. Status Solidi A **210**, 1264

(2013).
[43] X. Wu, F. Wang, and C. Wang, J. Magn. Magn. Mater. **384**, 40 (2011).
[44] M. E. Schabes and A. Aharoni, IEEE Trans. Magn. **23**, 3882 (1987).
[45] J. X. Zhang, PhD Thesis, Pennsylvania State University, U.S.A. (2008).
[46] X. P. Wang, Carlos J. Garcia-Cervera, and Weinan E, J. Comput. Phys. **171**, 357 (2001).
[47] T. Ando and T. Nishihara, IEEE Trans. Magn. **33**, (1997).
[48] N. Honda and K. Yamakawa, IEEE Trans. Magn. **50**, 3002504 (2014).
[49] J. U. Thiele, S. Maat, and E. E. Fullerton, Appl. Phys. Lett. **82**, 2859 (2003).
[50] S. I. Kiselev, J. C. Sankey, I. N. Krivorotov, N. C. Emley, R. J. Schoelkopf, R. A. Buhrman, and D. C. Ralph, Nature **425**, 380 (2003).
[51] J. S. Jiang, S. D. Bader, H. Kaper, G. K. Leaf, R. D. Shull, A. J. Shapiro, V. S. Gornakov, V. I. Nikitenko, C. L. Platt, A. E. Berkowitz, S. David, and E. E. Fullerton, J. Phys. D **35**, 2339 (2002).
[52] C. L. Platt, A. E. Berkowitz, S. David, E. E. Fullerton, J. S. Jiang, and S. D. Bader, Appl. Phys. Lett. **79**, 3992 (2001).
[53] K. N. Martin, K. Wang, G. J. Bowden, A. A. Zhukov, P. A. J. de Groot, J. P. Zimmermann, H. Fangohr, and R. C. C. Ward, Appl. Phys. Lett. **89**, 132511 (2006).
[54] D. Wang, A. R. Buckingham, G. J. Bowden, R. C. C. Ward, and P. A. J. de Groot, Proceedings-36th Annual Condensed Matter and Materials Meeting, WaggaWagga, NSW, Australia, 31 Jan.-3 Feb. 2012.
[55] G. B. G. Stenning, A. R. Buckingham, G. J. Bowden, R. C. C. Ward, G. van der Laan, L. R. Shelford, F. Maccherozzi, S. S. Dhesi, and P. A. J. de Groot, Phys. Rev. B **84**, 104428 (2011).